Assesment of the response of the meteorological/hydrological parameters on the soil gas radon emission at...

Article · July 2017

DOI: 10.1016/j.jseaes.2017.06.033

CITATIONS
0

READS
80

8 authors, including:

Baldev Raj Arora
Ministry of Earth Sciences,
131 PUBLICATIONS **1,022** CITATIONS
SEE PROFILE

Arvind Kumar
National Applied Research Laboratories
32 PUBLICATIONS **202** CITATIONS
SEE PROFILE

Vivek Walia
National Applied Research Laboratories
68 PUBLICATIONS **1,154** CITATIONS
SEE PROFILE

Tsanyao Frank Yang
National Taiwan University
168 PUBLICATIONS **2,177** CITATIONS
SEE PROFILE

Journal of Asian Earth Sciences xxx (xxxx) xxx–xxx

Contents lists available at ScienceDirect

Journal of Asian Earth Sciences

journal homepage: www.elsevier.com/locate/jseaes

Assesment of the response of the meteorological/hydrological parameters on the soil gas radon emission at Hsinchu, northern Taiwan: A prerequisite to identify earthquake precursors

Baldev R. Arora[a,1], Arvind Kumar[a], Vivek Walia[a,*], Tsanyao Frank Yang[b,2], Ching-Chou Fu[b,c], Tsung-Kwei Liu[b], Kuo-Liang Wen[a,d], Cheng-Hong Chen[b]

[a] National Center for Research on Earthquake Engineering (NCREE), NARL, Taipei, Taiwan
[b] Department of Geosciences, National Taiwan University (NTU), Taipei, Taiwan
[c] Institute of Earth Sciences, Academia Sinica, Taiwan
[d] Department of Earth Sciences and Institute of Geophysics, National Central University, Jhongli, Taiwan

ARTICLE INFO

Keywords:
Soil gas radon
Earthquake precursors
Meteorological/hydrological parameters
Ground water head
Singular spectrum analysis
Hsinchu
Northern Taiwan

ABSTRACT

The present study is an attempt to assess and quantify the influence of the meteorological (atmospheric temperature and pressure) and hydrological (rainfall and ground water head-GWH) parameters on the soil gas radon emission at Hsinchu, northern Taiwan. The quasi-periodic variations corresponding to diurnal and semi diurnal periods were estimated and eliminated by decomposing the time series for the period of September 16, 2009 to March 5, 2010 to singular spectrum analysis. The reconstructed non-periodic variations, which reproduce the salient feature of recorded time series, were searched for meteorological/hydrological influences in radon emission. The combined response of barometric pressure and atmosphere temperature are found to be small when compared to the total variability in radon. The influence of rainfall on radon is found to be strongest. At the onset of rainfall, radon shows a step-jump that attains peak with a time lag of 12–15 h. This enhancement is attributed to entrapment of soil gas in the top soil cover as increased soil moisture prevents escape of radon into the atmosphere (capping effect). The decay of radon after the recession of rainfall is approximated by double exponential decay terms, one corresponding to the natural decay of radon with half life of 3.84 days and second representing slow weakening of capping effect. The third effect related to internal loading due to rise and fall of groundwater modulates the propagation of radon in overlying strata, accounting for the long term variations in radon. The rainfall inflicted changes in radon look strikingly similar to earthquake related precursory or co-seismic perturbations, inferred by long term synotopic observations. It is surmised that unless radon variations are corrected for meteorological/hydrological contamination, some precursory signals are masked on one hand while on the other hand some anomalies are falsely viewed as earthquake precursors.

1. Introduction

As the stress level increases during earthquake preparatory cycle, the rocks in the impending focal zone experience opening of micro-cracks (Scholz et al., 1973). With the opening of cracks, exposed surface area of rocks also increases that leads to enhanced emanation of radon (Thomas, 1988). If this increase in radon intensity can be measured at the surface, it can serve as a possible precursor to earthquakes. With the realisation of the physical mechanism, some of the early field examples, e.g. 1966 M5,5 Tashknet earthquake (Ulomov and Mavashev, 1967), reporting several fold increase in radon in association earthquake occurrences has given major impetuous for initiating the monitoring of radon across the word wide seismic active (Barbosa et al., 2015; Heinicke et al., 1992; Igarashi et al., 1995; Virk et al., 2001; Steinitz et al., 2003; Zmazek et al., 2005; Kumar et al., 2009, 2015). So rapid is the growth, that number of reviews have appeared at regular time interval, attempting to characterize the nature of precursors, their physical validation or to establish a scaling relation of anomalous changes in radon with the magnitude and distance of impending earthquakes (Wakita et al., 1988; Thomas, 1988; Toutain and Baubron, 1999;

* Corresponding author.
E-mail addresses: arorabr47@gmail.com (B.R. Arora), vivekwalia68@gmail.com, walia@ncree.narl.org.tw (V. Walia).
[1] Present address: Uttarakhand State Council of Science & Technology, Jhajra, via-Premnagar, Dehradun 248007, India.
[2] Left for heavenly abode on March 12, 2015.

http://dx.doi.org/10.1016/j.jseaes.2017.06.033
Received 29 June 2016; Received in revised form 28 June 2017; Accepted 30 June 2017

Hartmann and Levy, 2005; King et al., 2006; Cicerone et al., 2009). Despite the rapid growth, yet no universal ones to isolate and document the diagnostic signature of a precursory signal in radon definition of earthquake precursory signal has emerged and hence radon precursors are seldom used in real time forecasting of earthquakes. Further, even if reported radon precursors are real, how they are physically related to the preparation process of an impending earthquake remain an open issue (Woith, 2015). More intriguing is the observation that there is apparent negative correlation between the numbers of reported anomalies and the length of the time series processed to isolate precursory signals (Woith, 2015). In other words, most of the so claimed success stories that have often emerged from short lengths of data and hence it is likely that influence of non-dynamic factors influencing radon variability may not be neutralised. However, as a result of continuing monitoring in different environments, it has been well recognised that the propagation and transportation of radon from the focal zone to surface is controlled by diffusion (gradient in concentration), advection (pressure- Clements and Wilkening, 1974), convection (temperature- Finkelstein et al., 2006) processes. In addition, modulation of soil moisture (capping effect- Schumann et al., 1988, 1992), squeezing of water (rinsing effect- Hesselbom, 1985) following events of rainfall produce strong contamination in radon intensity (Schumann et al., 1992; Fujiyoshi et al., 2006). The real assessment and quantification of these influences is a major pre-requisite to isolate weak precursory and co-seismic signals. The present study is a fresh attempt to quantify the nature and extent of influence of meteorological and hydrological parameter on radon emission in the seismically active belt of Taiwan, where dense network of soil gas radon monitoring network has been in operation for a long time (Walia et al., 2009a).

2. Monitoring network, data and synoptic observation

Fig. 1 shows the network of soil-gas monitoring stations in Taiwan, set up jointly by NTU-NCREE mostly as a part of sponsored projects of the Central Geological Survey of Taiwan. To build a monitoring station, reconstructions were done by digging holes of 2 m and by casing these holes with PVC pipes. At the bottom of PVC pipe, a fine mesh is attached to avoid the enterance of any unwanted materials into the pipe. The PVC sheet is put on all the sides of the PVC pipe at the bottom extending about 1 m on all sides; this avoids the rainwater to get into the hole. Some pebbles are also put at the bottom to minimise the meteorological effects before filling all sides of the holes. Finally the top surface is cemented and housing is build on it to keep the required instruments. Fig. 2 shows the sketch of the automated monitoring system. After passing through the water trap and gas cooler, the soil gas was transferred into an alpha spectroscopy (SARAD_RTM2100) via an internal pump for radon and thoron measurement. A two stage filter keeps out the radon and thoron progeny, only Rn-222 and Rn-220 gas can pass the chamber inlet. Radon counts per 15 min were recorded. The time interval of 15 min is long enough to yield count-sum well above the background noise level. All the data are transferred to the central processing office via the internet. Operation of stations commenced in a phased manner, data for the post-2006 are available in continuous mode, except for a short break due to malfunctioning of equipments or due to interruptions in power supply.

After careful examination of available data from network of 9 continuous monitoring stations, a segment of soil-gas radon data for the monitoring station Hsinchu (24.77 N 121.03 E) along the Hsincheng fault (Walia et al., 2009a), corresponding to period of August 11, 2009 to March 5, 2010, was selected. The continuity and regularity of the data was primary criteria to select this time window. The soil gas temperature, measured as a part of soil-gas station, was supplemented by allied meteorological parameters; namely barometric pressure, atmospheric temperature and precipitation (rainfall), recorded at a nearby site of national grid, operated by the Central Weather Bureau (CWB). The Hsinchu monitoring station was chosen especially because of the availability of con-current hydrological data in the form of the depth to ground water head in the deep bore-hole. Since allied

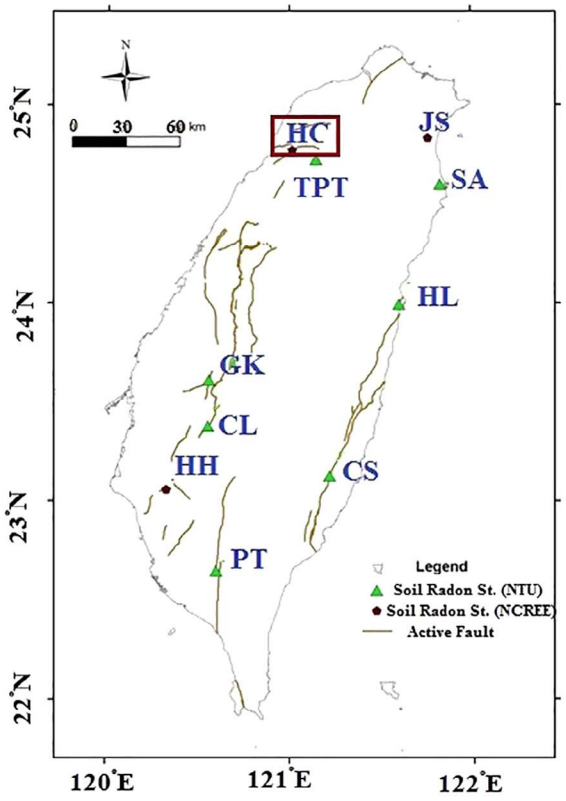

Station Name	Code	Institute
Hsinchu Station	HC	NCREE
Ta-ping-ti Station	TPT	NTU,CGS
Gu-Keng Station	GK	NTU,CGS
Chung-lun Station	CL	NTU,CGS
Hualien Station	HL	NTU,CGS
Hsin-hua Station	HH	NCREE
PT Station	PT	NTU,CGS
Chih-shang Station	CS	NTU,CGS
Su-ao Station	SA	NTU,CGS
Jiao-si Station	JS	NCREE

Fig. 1. Network of soil-gas (radon) monitoring stations in Taiwan, set up jointly by NTU-NCREE, largely with financial support projects from the Central Geological Survey (CGS). Radon data of station Hsinchu (HC) in the northern part of Taiwan is used in the present study.

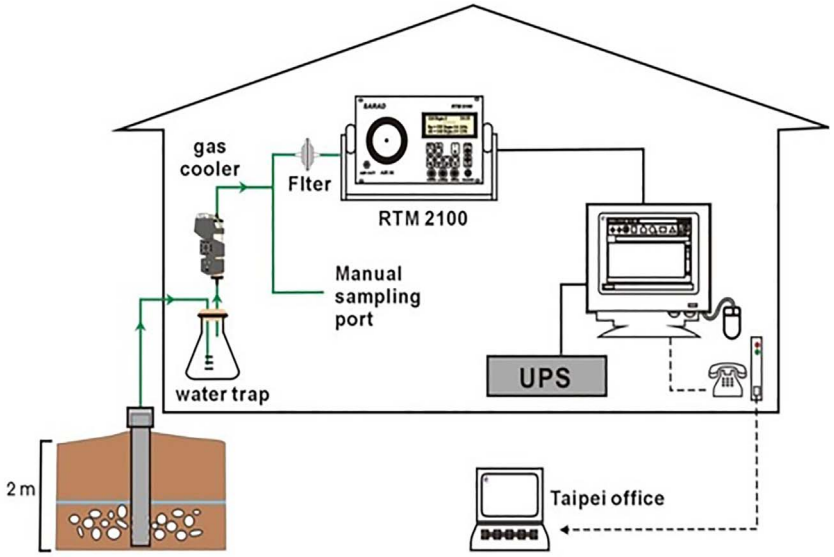

Fig. 2. Sketch of the automated soil gas monitoring station. Soil gas picked from 2 m deep pit, Alpha spectrometer (RTM2100) is used to measure Radon (Rn-222) and thoron (Rn-220) gas.

meteorological and hydrological data were available with hourly sampling, 15-min radon were also reduced to hourly sums. It was noted that certain selected time-series, e.g. ground water head (GWH) and meteorological parameters, are dominated by varying degree of long term trend (especially GWH) and seasonal variations. Since, the primary objective here is to search short-term changes (of the order of a few days to 15–20 days) related to earthquake occurrences, variations with periods longer than 30 days were eliminated by subjecting each time series of hourly values to digital Butterworth filter. Fig. 3 gives the time plot of filtered soil gas radon (simply referred as radon in the rest of the manuscript) together with allied meteorological and hydrological parameters. The comparison of soil temperature with atmospheric temperature data collected from the CWB showed complete agreement in their time variability, ensuring compatibility and, thus, validating the use of data from closely spaced CWB sites (Fig. 3). The bottom panel in Fig. 3 depicts occurrences of earthquakes of $M \geq 5$ within the radius of < 150 km of the station Hsinchu. The origin time, location and magnitudes of the earthquakes were extracted from the catalogue of the CWB (www.cwb.gov.tw).

3. Pre-processing of data

3.1. Single Value Decomposition (SVD)

It was observed that filtered time series for different parameters are dominated by two classes of time variations; (i) periodic variations at diurnal frequencies, (ii) aperiodic signals with time scale of 2–30 days, later determined by the cut-off period of filter applied. In addition, different time-series are superposed with varying levels of random/white noise. To extract main patterns present in each parameter, we took recourse to data-driven Singular Spectrum Analysis (SSA) technique that has the potential to isolate periodic and aperiodic signals without prior knowledge on the dynamics of the composite time series (Broomhead and King, 1986; Vautard et al., 1992). In this technique, the separation of time varying patterns are obtained by diagonalizing the empirical covariance matrix; the physical rationale. Alternative formulations used to construct the covariance matrix are described in the series of papers (Broomhead and King, 1986; Vautard and Ghil, 1989; Vautard et al., 1992; Plaut and Vautard, 1994; Allen and Robertson, 1996; Ghil et al., 2002). In the present study, we adopted the numerical algorithm proposed in Vautard and Ghil (1989; also see Vautard et al., 1992) as it allows extraction of dominant waveforms with improved noise reduction, particularly when applied to short time series (Ghil et al., 2002). Implementation of algorithm begins by organizing lagged co-variances (auto variance) with a maximum lag of M into a matrix, which has Toeplitz structure i.e., constant diagonals corresponding to equal lags as follows:

$$\frac{1}{M}\begin{vmatrix} \rho_0 & \rho_1 & \rho_2 & \cdots & \rho_{M-1} \\ \rho_1 & \rho_0 & \rho_1 & & \rho_{M-2} \\ \cdots & \cdots & \cdots & & \cdots \\ \rho_{M-1} & \rho_{M-2} & & & \rho_0 \end{vmatrix}$$

Next, lagged covariance matrix is subjected to eigen value decomposition (EV) to obtain the eigen values (λ_k) and eigen vector (τ_k). These are then sorted in descending order of the magnitude of λ_k, where index $k = 1, 2, \ldots, M$. Finally, the resolved eigen vectors and eigen values are used to reconstruct the time evolution of the kth component over the length of the original time series. Reconstructed components (RCs) corresponding to increasing values of index k is analogous to the principal components present in the time series in order of descending amplitude. In principle, reconstructed component (RC) can be computed for each value of index k but in practice it is found that limited number of eigen values with descending amplitude collectively reproduce the salient feature of the time series. The relative contributions of the individual components to the total variance of the filtered time series (subjected to the SSA) are obtained so that computation could be restricted only to significant components.

3.2. Application of SSA and results

The implementation of the adopted SSA algorithm intricately relies on the use of Fast Fourier Transformations (FFT) and this necessitated the length of processed time series to be some power of 2. To meet this requirement, time section corresponding to a length of 4096 h starting with the midnight of September 16, 2009 was used. The choice of lag-window size, M, is trade off between the spectral resolution versus the degree of statistical confidence in the information resolved (Ghil et al., 2002). Larger M ensures higher spectral resolution, but statistical stability is better with smaller M-point window (see Chen et al., 2013 for discussion on the choice of the size of M). To meet this contrasting requirement, M should neither be too large nor too small in respect to the total length of time series (N), invariably M not exceeding N/5 (Vautard et al., 1992). After initial trial experimentation, it is found $M \sim 300$ extracts dominant patterns coherent to individual time series.

3.2.1. Decomposition of time varying fields into periodic and aperiodic signals

As an example of the application SSA to present data sets, we show

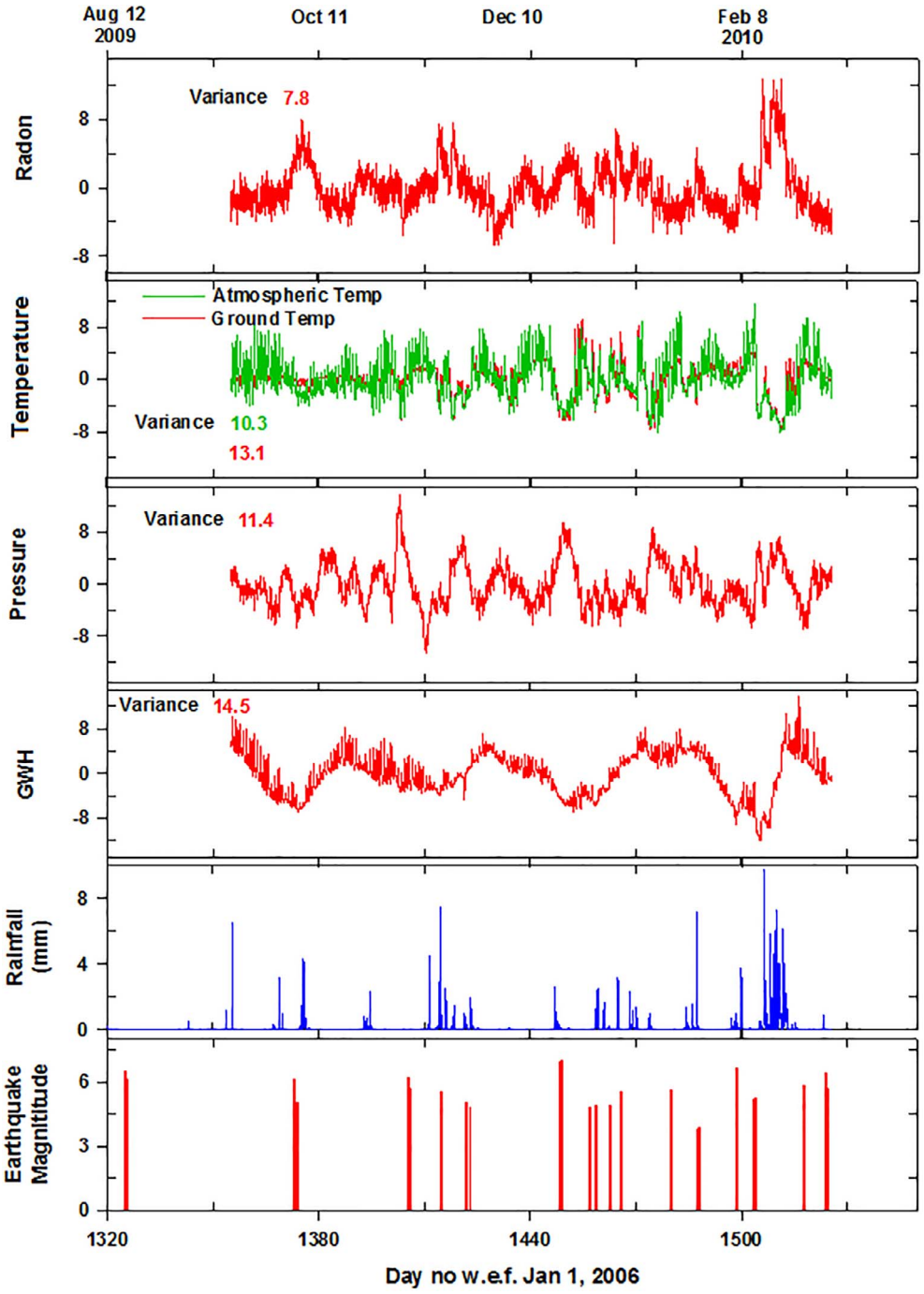

Fig. 3. Plots of high pass filtered hourly time series of radon, Ground Water Head (GWH) and allied meteorological parameters, showing variations with periods < 30 days at station Hsinchu for the period of August 11, 2009 to March 5, 2010.

reconstructed time variations corresponding to first 4 EVs in radon time series (Fig. 4). As noted, the first group represented by EV-1 and EV-2 represents dominantly aperiodic components, which together account for nearly 68 percent of variance. The second group denotes periodic variations. FFT indicates that periodic variations correspond to diurnal and semi-diurnal periods. However, these periodic EV-3 and EV-4 together account for less than 2 percent of variations of initial data free from long term seasonal variations. Interesting aspect is that sum of just first two EVs are able to reproduce the most salient features of the total observed variations (lower panel in Fig. 4). More significant is that synthesized variations are largely free from the random and white noise, later accounting for nearly 30 percent of the total variability (Fig. 4).

The applications of SVD to hydrological and meteorological (GWH and temperature/pressure) data has shown time variations in each parameter and are composed of dominantly aperiodic and quasi-periodic variations. As an example, Fig. 5a, b shows the nature of decomposed time variations respectively in aperiodic and periodic signals for short time segment of 60 days, i.e for day no. of 1400–1500 w.r.t Jan 1, 2006 whereas Fig. 6 gives sum plot of decomposed aperiodic variations in different parameters together with rainfall spells and earthquake occurrences. The relative strength of the dominant EVs defining the aperiodic and periodic variations in different parameters is given as the percentage variance accounted by respective components (Table 1). Percentage variations are obtained by normalising the variance of each EVs with respect to the total variance of filter time series in respective parameters, given in Table 1.

3.2.2. *Characteristic of periodic signals*

Like radon, periodic variations accounted only 1–2 percent of the

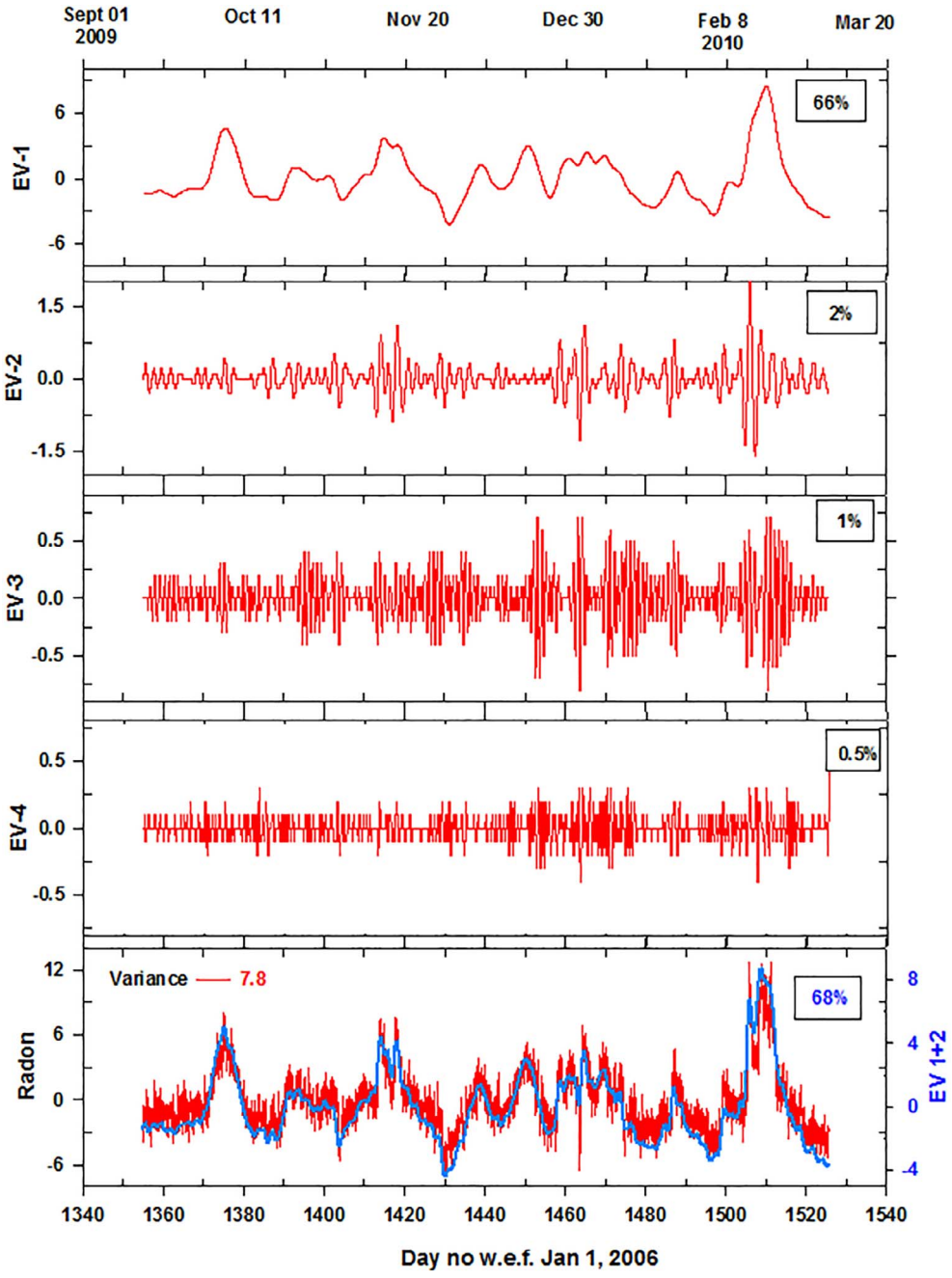

Fig. 4. Time plots of decomposed Eigen Values (EV) corresponding to dominant aperiodic (EV1 & EV2) and periodic (EV3, EV4) components in Radon at station Hsinchu during September 16, 2009 to March 5, 2010. Percentage variance accounted for by individual EVs and the aperiodic component are also indicated on the side.

total variance in barometric pressure and GWH. However, the periodic variations in atmospheric temperature account for higher variance of 6 percent of the total variations (Table 1). Time evolution in GWH head is dominated by daily variations and also show long term modulations. Presence of strong variations corresponding to lunar diurnal (24 h 53 m) and semidiuranal periods coupled with superposed lunar semi monthly modulations are considered diagnostic characteristic of deep seated confined aquifer (Matsumoto, 1992). Spectral analysis of periodic variations in water head for full time series as well as for smaller segments using FFT as well as MEM (Maximum Entropy Method) spectra does not favour lunar tidal origin for the observed variations in GWH at the present observation site. Instead, the anti-phase correlation of daily variations in GWH and temperature suggest that underground water head is sensitive to external atmospheric thermal/pressure loading. Another noteworthy observation is that rhythmic daily variations in the GWH, radon and temperature are synchronously perturbed with the spells of rainfall. These local perturbations in the temperature and GWH can be related with the weather pattern modulating temperature/pressure and causing rainfall.

3.2.3. *Characteristic of aperiodic signals*

The influence of external atmospheric temperature/pressure as well as rainfall are also well documented in the strong aperiodic signals in the radon and the GWH (Figs. 5a and 6). It is seen that continuous varying aperiodic signals in radon, representing quasi-periodic variations with periods ranging between of 8–12 days, appear to be correlated with changes in temperature and pressure, the later two showing almost linear inverse relation. The influence of rainfall on aperiodic variation in radon have more distinct changes. As seen in Figs. 5a and 6 that following each rainfall sequence, there is rapid increase in radon intensity attaining peak with time lapse of 12–18 h. The calculation of lagged correlation between rainfall sequence and radon variations (Fig. 6 – top panel) imply that radon variations attain peak after a time lag of 15 h following rainfall occurrence. This property is later used to

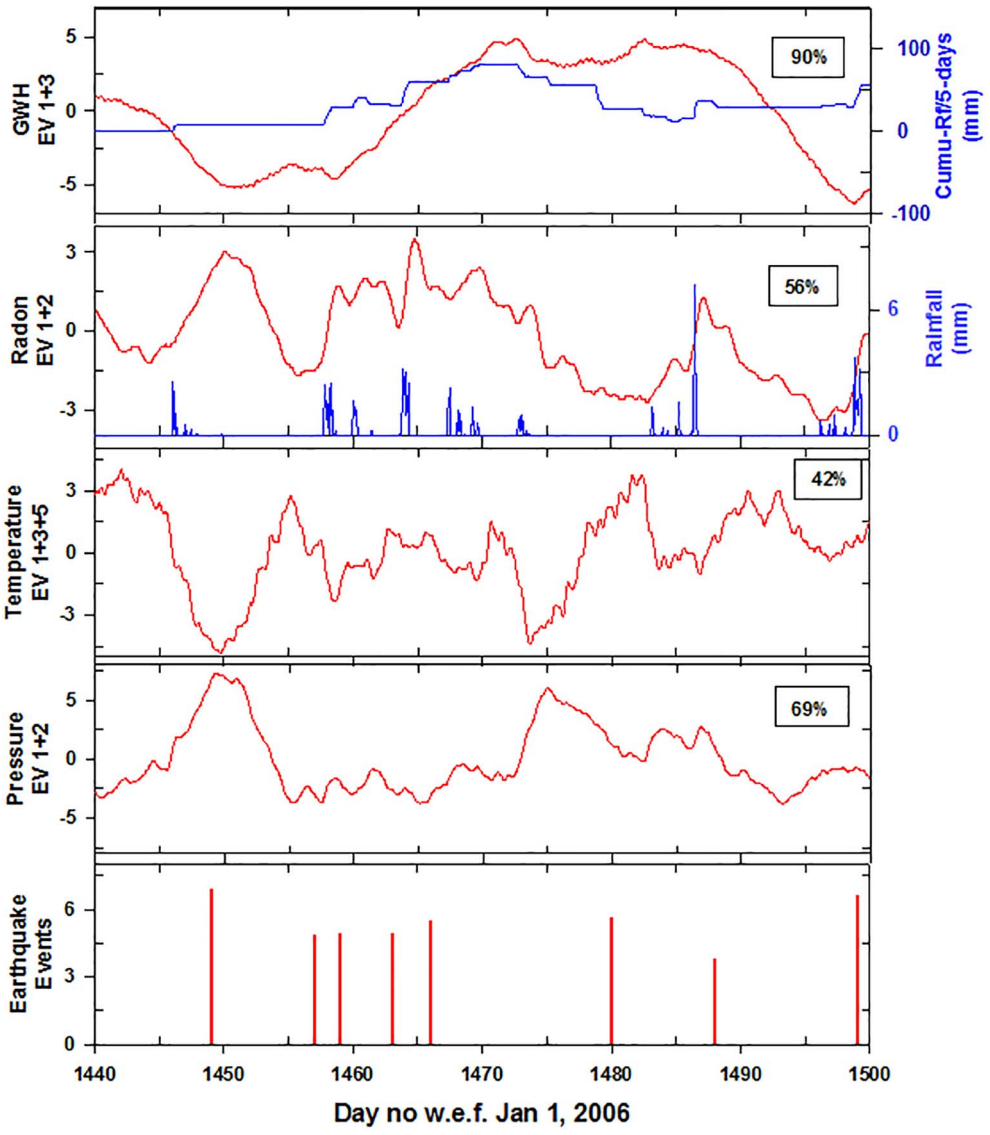

Fig. 5. Time plots of reconstructed (a) aperiodic and (b) periodic components in the Ground Water Head (GWH), Radon, Atmospheric Temperature and Barometetric Pressure at Hsinchu, for shorter segment, corresponding to day No. 1440–1500, of the total length of data processed in the present study. Percentage variance accounted for by the aperiodic and periodic components in different parameters are also included in respective plots. Histograms within select panels the show distribution of Rainfall (Rf). Blue curve along with the plot of the GWH variation in (a) shows the variation in cumulative rainfall during 15 days preceding any given day (extracted from Fig. 7). Lower panel shows the timings of M > 5 earthquakes during the period of observations.

simulate quantitively the step rise in radon following precipitation.

Given earlier inference that underground water fluctuations do not portray characteristic of confined aquifer, the GWH should be a better candidate to respond to sporadic events of rainfall. However, the observed GWH variation does not depict any sharp changes to rainfall sequences. It follows from Figs. 6 and 7 (top panel) that the GWH during prolonged dry spells, i.e. in between two successive spells of rainfall is continuously declining. Following heavy spells of rainfall, GWH begins to rise, rather slowly to reach peak after several days of the recession of rainfall activity. Such inference is corroborated when the changing water level are correlated with accumulated rainfall for the duration of 2, 5, 8, 10, 15 days (Fig. 7). The plot showing accumulated rainfall over 10–15 days mimic fairly well the variations in ground water level (Fig. 7). These features suggest that the aperiodic rise and fall of ground water level is apparently controlled by the recharge and discharge of subsurface aquifer wherein the process of recharging at the onset of precipitation, but bulk recharge continues for longer duration of 10–15 days following the recession of rainfall. Rate of rise being dertemined by the lithology/porosity of rocks controlling the percolation of rainwater as well as by surface runoff contributing to the recharge of acquifer. The decreasing rate in GWH during the dry spell would be a function of processes controlling the discharge of the acquifer, including thermal evaporation of moisture from surface soil cover, which would vary with rainfall intensity and distribution.

4. Estimation of the influence of meteorological and hydrological parameters on radon emission

From the above decomposed aperiodic variations, it follows that the influence of rainfall and allied meteorological parameters vary greatly on affected parameters, e.g. while the response of radon emission to rainfall is characterized by step rise and complex decay pattern, the GWH, temperature/pressure are marked continuous rise (loading) and decline (unloading) with varying phase lags/delays. Hence, any technique adopted to estimate the hydrological and meteorological parameters should take cognizance of these features and should also weigh the likely physical mechanisms.

4.1. Influence of temperature/pressure on radon intensity

Bayesian Tidal Analysis Program in a Grouping Method (BAYTAP-G) was originally developed to compute the response of GWH to the changing barometric pressure as well as to compute the contribution from earth tides (Tamura et al., 1991) A significant merit of the BAYTAP-G formulation is that it does not assume that the cause-effect (say the influence of pressure on on radon) is time synchronous but any effect of the change in influencing parameter (say pressure) may persist on the future measurements of affected parameter, in our case radon. Taking advantgae of this feature we estimate independently the

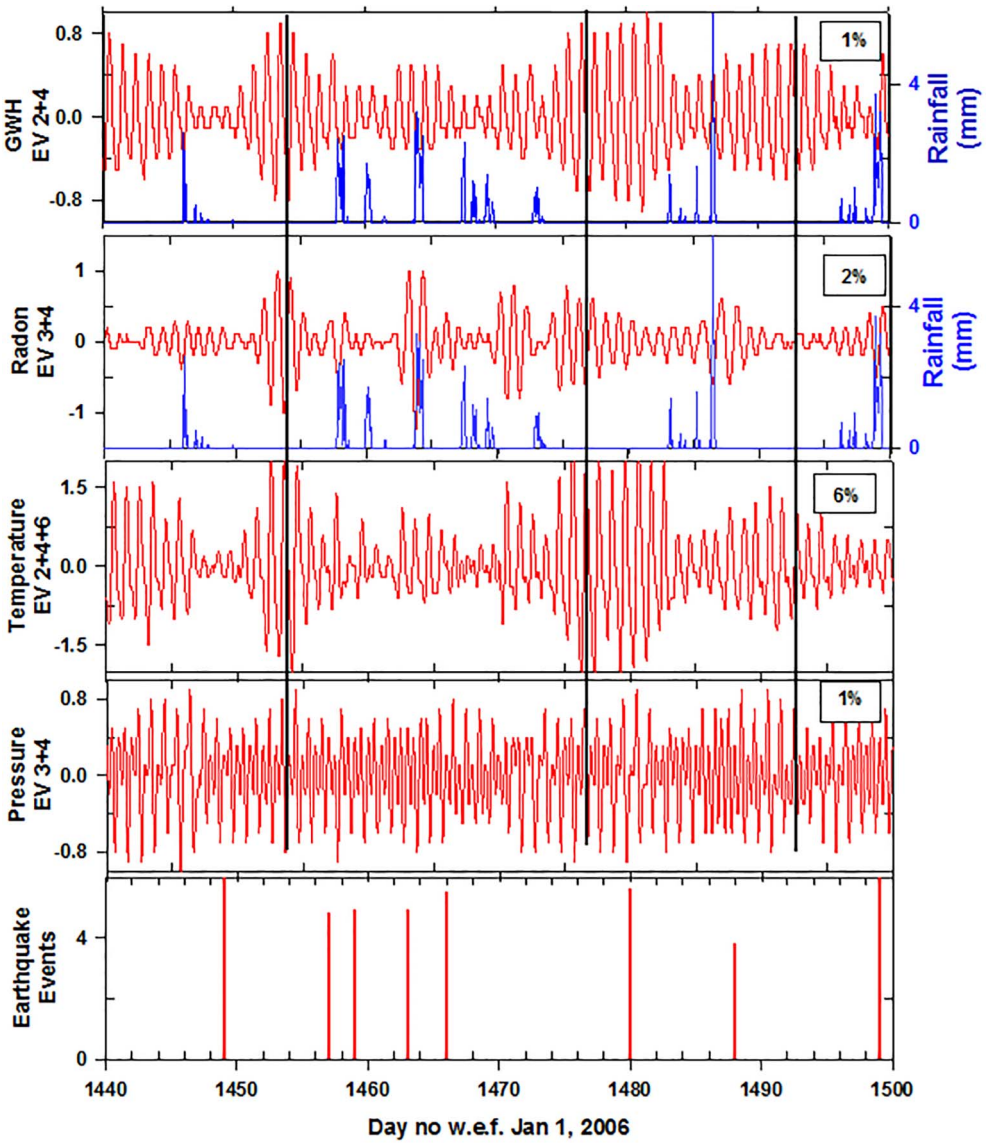

Fig. 5. (*continued*)

influence of continuous loading/unloading of temperature and pressure on radon variations, using the BAYTAP program available for use in the public domain on the website of the Geological Survey of Japan (http://riodb02.ibase.aist.go.jp/db086/GSJ_E/water/analysis/). In its adoption here, the delayed response on an affected parameter (radon) is recovered by using lagged auto regression terms as follows:

Pressure Induced Response (PIR)

$$P_n = \sum_{i=0}^{l=25} a_i \; p_{(n-i)} \tag{1}$$

Here, p_n is observed barometric pressure

Temperature Induced Response (TIR)

$$Te_n = \sum_{i=0}^{l=25} b_i \; te_{(n-i)} \tag{2}$$

Here, te is observed temperature

Prior to applying of BAYTAP-G to the data, calculation of lagged correlation between radon independently with temperature and pressure show that correlation peak within short time-lag window of ± 7 h and then drop down to statistically insignificant level within the time lags of 25 h (top panel in Fig. 6). In agreement with this, stable effect of pressure variations on radon were recovered when the cumulative effects of pressure for the past 25 h were considered in Eq. (1). Any change in lags between 12 and 36 h did not alter the nature of pressure induced effects on radon in any significant manner. Similarly, treating temperature as an independent parameter, its influence on radon were estimated using 25 lagged terms. It is apparent from Fig. 8 that like the decomposed aperiodic component in radon (red curve in upper panel), pressure/temperature inflicted changes in radon (blue and green curves in middle and lower panel) are negatively correlated with temperature (lower panel in Fig. 8)) but positively correlated with pressure (middle panel in Fig. 8). Since the temporal progressions in pressure and temperature are not independent of each other but show strong anti-phase correlation (correlation coefficient of −0.61), it's hard to conclude whether radon variability is controlled by either temperature or pressure variations. This ambiguity is resolved with recourse to computation of total and partial correlation. Computation of partial correlation allows to examine the correlation of one parameter with other by mathematically neutralizing the effect of variability of third parameter constant. It is found that a direct correlation between aperiodic variations in radon and pressure is statistically significant with a value of 0.48 but when the influence of accompanying variations in atmospheric

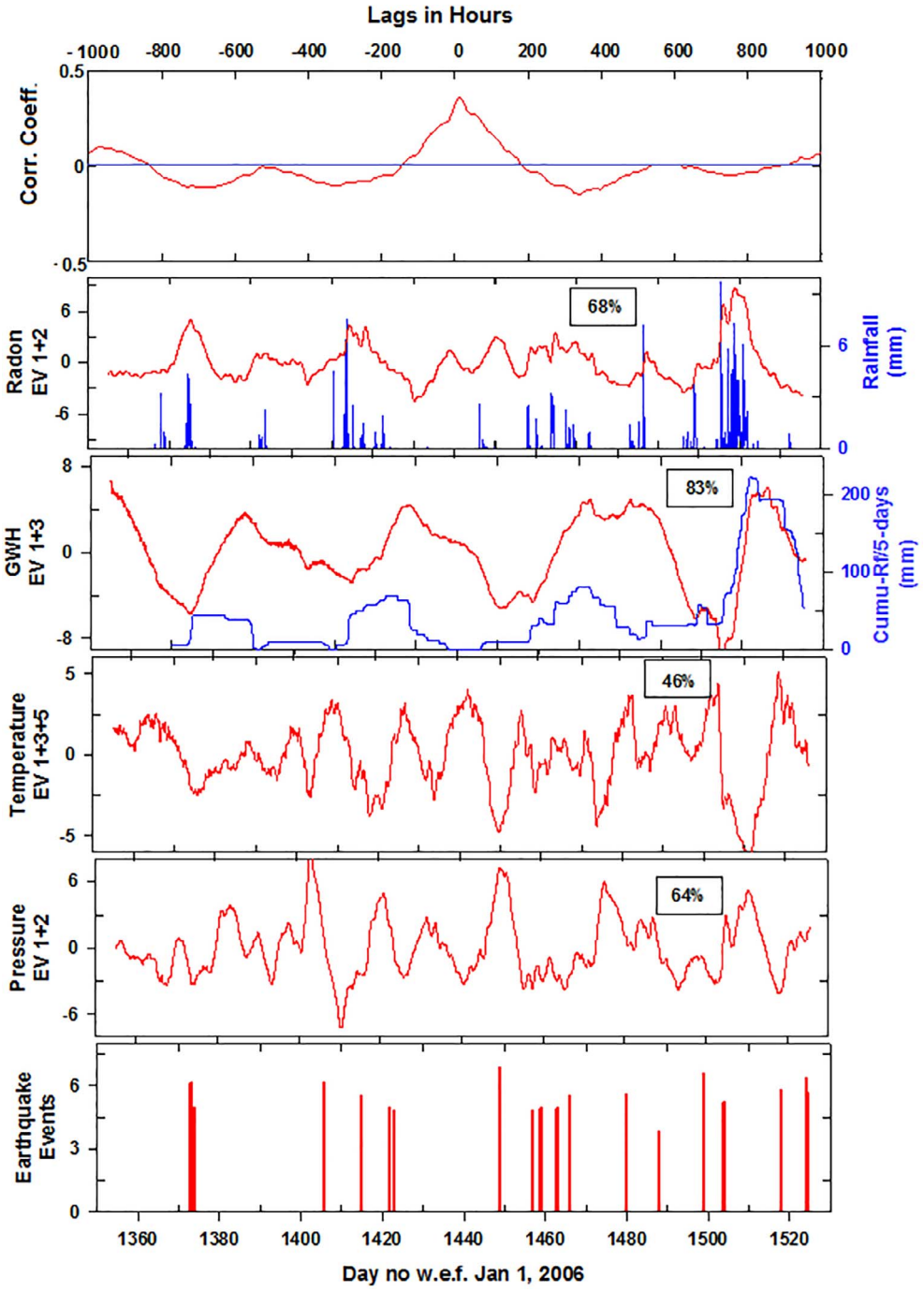

Fig. 6. Plots of reconstructed aperiodic components in Ground Water Head (GWH), Radon, Atmospheric Temperature and Barometetric Pressure at Hsinchu, for the period of September 16, 2009 to March 5, 2010. Percentage variance accounted for by the aperiodic component in different parameters are also indicated. Histograms within radon panel shows the distribution of Rainfall (Rf). Blue curve along with the plot of GWH variation shows the variation in cumulative rainfall during 15 days preceding any given day (see Fig. 7). Lower panel shows the timings of M > earthquakes during the period of observations, whereas top panel gives lagged correlation coefficient between Rainfall and Radon.

Table 1
Percentage variances accounted for by the decomposed Eigen Values (EV) in Radon, Ground Water Head (GWH), Atmospheric Temperature and Pressure at Hsinchu, northern Taiwan.

Parameters	Variance-Filter	% Variance-APERIODIC[a]			% Variance-PERIODIC[a]			Sum APERIODIC + PERIODIC (total)
Radon	7.8	EV1	EV2	Sum	EV3	EV4	Sum	70
		66	2	68	1	0.5	1.5	
GWH	14.5	EV1	EV3	Sum	EV2	EV4	Sum	85
		82	1	83	1.5	0.5	2	
Temperature	10.3	EV1	EV3	Sum	EV2	EV4	Sum	53
		44	2	46	6	1	7	
Pressure	11.4	EV1	EV2	Sum	EV3	EV4	Sum	66
		63	1	64	1	0.5	1.5	

[a] Percentage variations are obtained by normalizing the EV with respect to the variance of filtered time series of respective parameter.

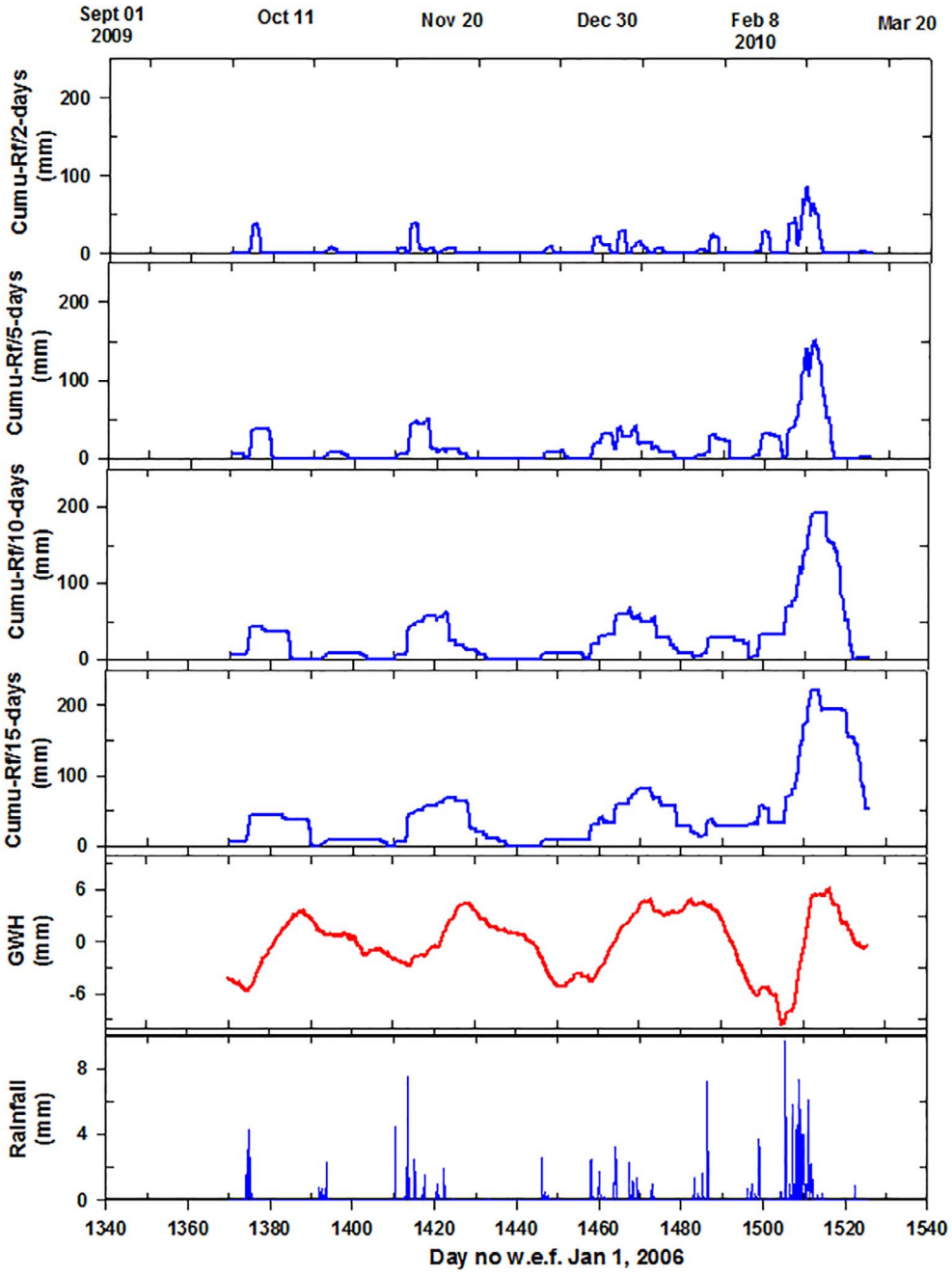

Fig. 7. Plot showing time variation in cumulative rainfall successively summed over intervals of 2, 5, 10 and 15 days preceding together with variation in GWH (red curve) at station Hsinchu during September 16, 2009–March 5, 2010. Lower panel shows the distribution of rainfall (Rf). (For interpretation of the references to color in this figure legend, the reader is referred to the web version of this article.)

temperature is neutralised, the partial correlation drops to a statistically insignificant low value of 0.06. In contrast, strong direct negative correlation between radon and temperature (−0.45) persists even when influence of contemporary variations in pressure is eliminated. This allows to surmise that noted dependence of radon on pressure variation is the pseudo effect arising largely due to the interrelation between temperature and pressure. However, significant partial correlation of −0.38 warrant that ~14% of the radon variability (square of partial correlation multiplied with 100) is inflicted by the variation in temperature alone. This is good agreement with the results of BAYTAP-G which show that variance of aperiodic radon variations (0.5.31) when corrected for temperature inflicted variations (green curve in upper panel of Fig. 8) reduces to 4.73, permitting an inference that only about 11% of the variability in radon is due to the changes in atmospheric temperature.

4.2. Quantification of Rainfall Inflicted Response (RIR) in radon variations

It is already noted that radon variations exhibit a steep-rise attaining peak with a time lag of about 15 h after the occurrence of rainfall sequence (Figs. 5a and 6). After the recession of the rainfall, radon variations decay in a rather complex manner till the next spell of rainfall. Therefore, the quantification of the rainfall influence on radon variability basically reduce to simulating a sharp increase and return to prevailing background variations.

4.2.1. Simulation RIR in radon by tank model

Analogous to radon intensity, gravity as well as GWH are prone to stress build up during earthquake cycle and are also shown to vary during long spells of rainfall (Imanishi et al., 2006; Matsumoto, 1992; Matsumoto et al., 2003). Controlled source experiments as well as numerical techniques are proposed to simulate and clean the data for rainfall-induced-responses (Naujoks et al., 2010; Nawa et al., 2009;

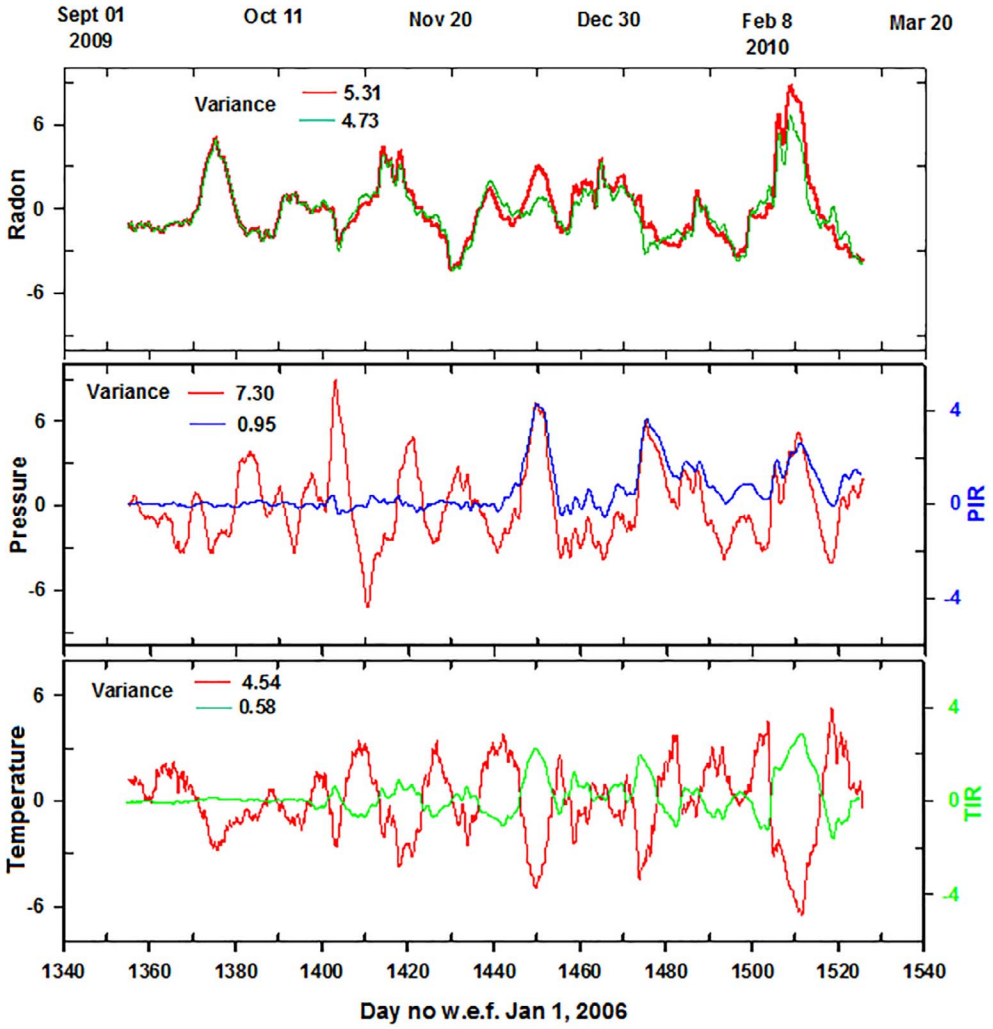

Fig. 8. Lower two panels respectively show temperature (green) and pressure (blue) inflicted changes in radon in relation to atmospheric temperature and barometric pressure (red), calculated using BAYTAP-G algorithm developed by Tamura et al. (1991). Upper panel shows radon variations corrected for temperature (green) inflicted changes in relation to aperiodic variations in Radon (red). Variance of respective curves are also indicated. (For interpretation of the references to color in this figure legend, the reader is referred to the web version of this article.)

Matsumoto et al., 2003). The tank model is one good example, which has been used successfully to simulate rainfall induced gravity variations (Nawa et al., 2009). Under the assumption that processes controlling RIR in radon are similar to gravity field, we test applied the tank formulation to simulate variations in radon due to rainfall occurrences. In the tank formulation, the radon change R(t) due to rainfall (Rf) is described by the differential equation

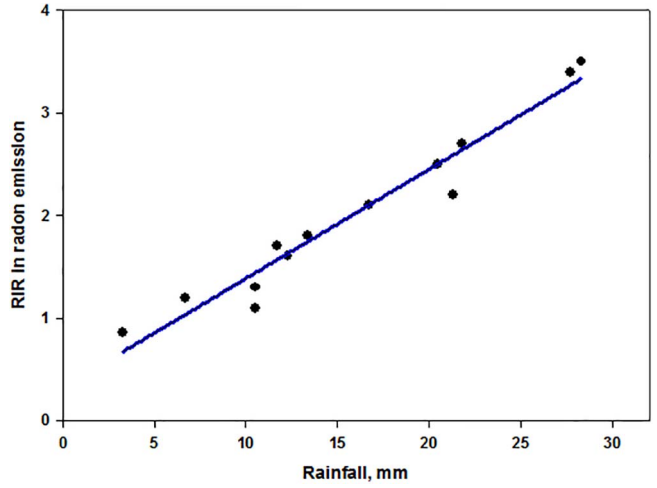

Fig. 9. Plot showing linear relation between sequences of cumulative rainfall and magnitude of step rise in radon emission.

$$\frac{dR(t)}{dt} = \gamma\Theta(-R(t)) + \alpha\, Rf(t) \tag{3}$$

where Rf (t) is the rainfall rate at time t, measured here by rainfall per hour (mm/h). α is a constant of proportionality between rainfall and radon, and γ represents the radon recovery rate after rainfall, and Θ is a Heaviside step function. As rainfall is often not a single spell, but occurs in spells in short succession lasting over from a few hours to a couple of days. Bunching of rainfall spells is a conspicuous feature of rainfall distribution all over the total study period (Fig. 6). Net consequence is that the magnitude of step jump is a measure of the cumulative response of spells in each individual bunch. This preposition is well supported by the scatter plot between the amplitude of net change in radon in response to sum of precipitation in individual bunch (Fig. 9). The high degree of linear fit is consistent with Eq. (1) and suggests that the constant of proportionality (α) between precipitation and radon is given by the slope of the best fitting line. Since the linear increase in radon to individual spell of rainfall continues to rise for about 15 h, RIS in radon at any given time (t) is given by the cumulative sum of precipitation over the past 15 h as follows:

$$RIS(t) = \sum_{k=0}^{15} \alpha' Rf(t-k) \tag{4}$$

α′ is constant of proportionality normalised to represent an increase per hour.

Again in agreement with equation, radon decay immediately following rainfall is considered to decay linearly with time. The decay constant (γ) in the tank model is estimated from trial and error

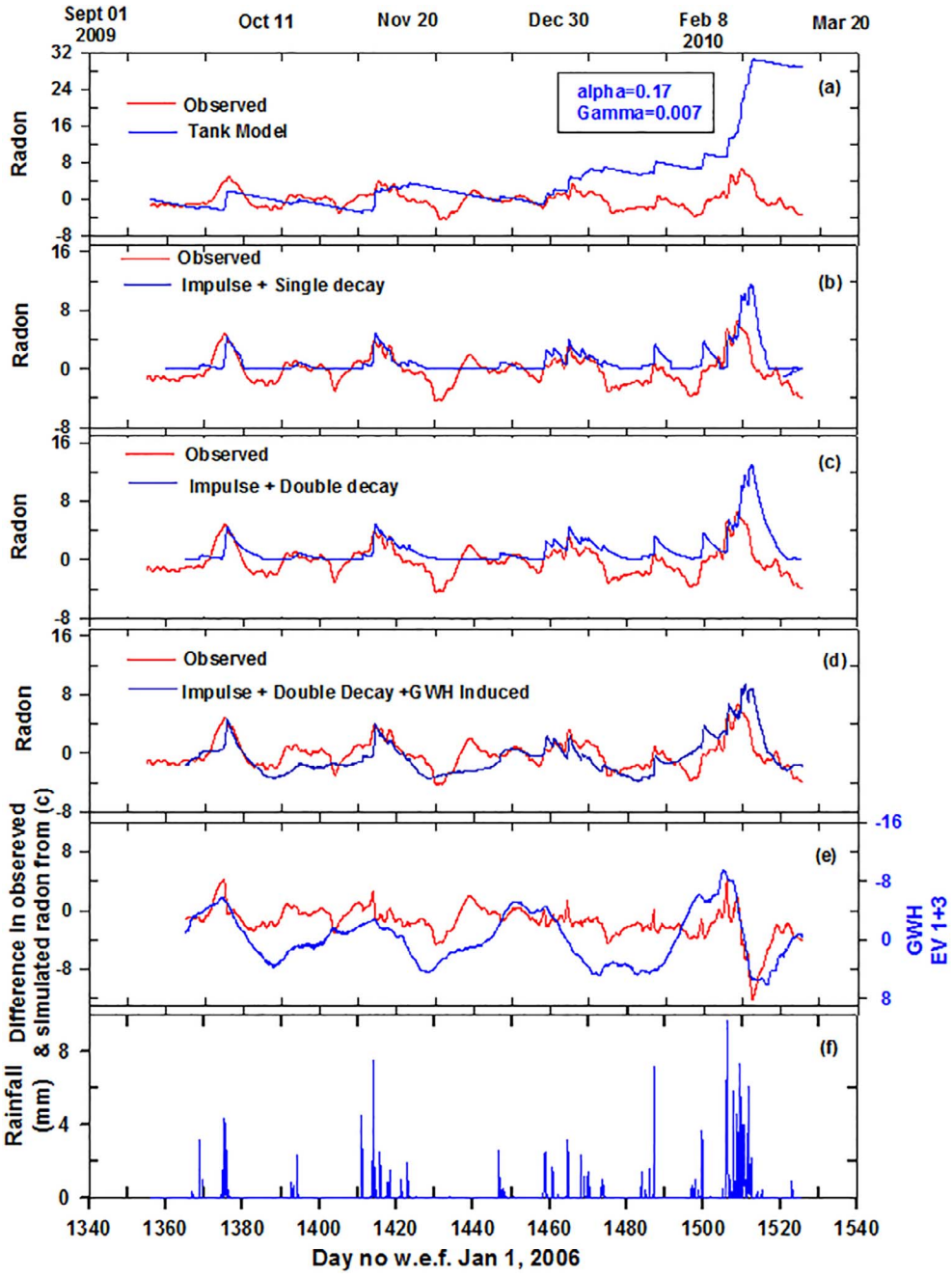

Fig. 10. Decomposed temperature compensated aperiodic radon variations (red), and predicted rain inflicted steep rise and follow up recovery decline simulated differently (a) by Tank Model; (b) exponential decay; (c) double exponential decay simulating respectively natural decay with half life of 92 h and second associated with the weakening of capping effect (half life equal to 240 h) and (d) double decay together with internal loading due to rise and fall of ground water head (see text for details). Panel 'e' give the plot of residual radon obtained differencing the aperiodic component (red curve) and simulated radon (blue curve) in panel 'd' in relation to the reversed plot of GWH variation. Lower panel 'f' shows the distribution of rainfall (Rf). (For interpretation of the references to color in this figure legend, the reader is referred to the web version of this article.)

adjustments to the decreasing trend in radon following each rainfall sequences. Fig. 10a shows the observed and predicted values of radon obtained by substituting the data based estimated constants ($\alpha = 0.17$; $\gamma = 0.007$). It is found that magnitude of estimated step rise, following individual rainfall events, are excellently well reproduced though the linear decay between successive rainfall sequences does not simulate the observation satisfactorily.

4.2.2. Simulation of RIR in radon with exponential decay term

The failure of the Tank model to approximate rain-induced variability in radon, led us to try an exponential mode of decay in radon following rainfall events. The latter has been shown to explain the nature of the variations in ground water level after the rainfall sequences in the tectonic setting of Taiwan (Jan et al., 2007). In its adoption, the radon following steep rise is assumed to decay exponentially by varying weighting factor. Radon intensity (RI) at time 'I' is estimated by:

$$RI_i = \sum_{j=0}^{n=120} \alpha w(j) Rf_{i-j} \quad (5)$$

where $w(j) = \exp(-j\beta/\Delta T)$.

Here α is weighing factor at time j before the rainfall impulse at time i. β is the exponential decay weighting factor to be determined empirically (estimated as -0.25) and T is the time interval in hours for the radon intensity to drop to half of its peak amplitude (after trial T was fixed at 120 h). Comparison of observed and predicted response adopting $\beta = -0.25$ and T = 120 h showed that both rise and initial fall were satisfactorily reproduced for the time window of the order of 100 h from the onset of rainfall. However, in the later part predicted trend is nearly flat and does not simulate the observed lower decay rate in the late time window (Fig. 10b). Even when high values of T (240 h) were tested, the observed trend could not satisfactorily reproduce decaying tend in the late phase.

4.2.3. Simulation of RIR in radon by including double exponential decay terms

With a rational to draw numerical strategy to completely explain the time evolution of radon-rainfall linkage, we afresh list major diagnostic and likely operating physical mechanisms:

(i) Pre-rainfall phase: During dry period, there is a free exchange of radon from soil to atmosphere and vice versa, and radon level at this stage represents the normal intensity determined by rock types/lithology of the measuring site.
(ii) As rainfall starts, soil gets moist and escape of radon from soil to atmosphere and visa a verse is inhibited, leading to radon accumulation beneath the thin cap of moist soil. Such mechanism, termed as capping effect (Schumann et al., 1988), would account for the observed sharp increase of radon following the rainfall spell.
(iii) Following the recession of rain, weakening of capping effect will cause decay of radon. The weakening of capping arises either due to evaporation of moisture from top soil cover or by hydrological factors facilitating the expulsion (squeezing) of water from upper strata. The term 'rinsing effect' was introduced by Hesselbom (1985) to account for the decay of radon soon after the recession of rainfall spells. In such cases, the rate of decay would be determined by porosity, fracture density, soil type and prevailing temperature conditions, etc.
(iv) In contrast to the geophysical parameters, e.g. gravity, water level, radon is naturally radioactive gas which decays exponentially with a half life of ~92 h. Any temporal increase in intensity, say by capping effect, would be followed by natural exponentially decay with a half life of ~92 h.

In the background of these physical considerations, the revised numerical scheme applied to account for the decay pattern of radon included a pair of exponential decay terms, one corresponding to natural decay with T = 92 h and the second representing weakening of capping effect after the rainfall. The double exponential terms, similar to Eq. (2) reproduced the most salient decreasing behaviour, both in the early and late time window (Fig. 10c). In the initial 100 h or so, both exponentially falling intensities combine to produce the steep drop of radon during the early phase (~100 h) whereas in the later phase decay pattern of second exponential function with T = 240 h trace the slow decay of radon intensity (Fig. 10c). It also emerges that in the late extended phase, radon variations fall in-line with the pre-rainfall level. However, during this intervening periods in between two spells of rainfall, the observed radon values show significant negative excursions with respect to the predicted trend (Fig. 10c). Since the decay pattern obeying exponential decay law will never drop below the pre-rainfall level, the negative field excursion suggests contributions from other sources. In fact, difference plot between observed and predicted trends is dominated by some smooth long term variations which with large phase shift appear to be replica to variation in water head recorded near the radon monitoring site (Fig. 10e). It has been already shown that ground water fluctuations are delayed phase response to rainfall activity (Fig. 7). This rise and fall of ground water could serve as an extra internal load on the radon concentration embedded in the overlying soil column, where the degree of saturation itself will vary with rainfall distribution. Taking rare advantage that in addition to radon intensity, information on water level variations is available by the in-situ measurements, the effect of internal loading on the radon concentration embedded in the overlying soil column was estimated using the regression terms with large lags, similar to Eq. (1). This factor was critical in accounting the relatively smooth long term variations in radon, including negative excusions in between the prolonged interval of no rainfall (Fig. 10d). In sum up, physical processes simulating overall rainfall inducted response (RIR) in radon can be expressed as sum of following effects: The capping effect accounting for the steep rise immediately following the rain; Double decay terms, one corresponding to natural decay of radon with T = 92 h and second exponential decay with T-240 representing weakening of capping effect and internal pressure loading arising due to rise and fall of ground water level accounting for long term variations in radon, especially reduction during long pauses in rainfall (Fig. 10d).

5. Discussion

5.1. Overview of the influence of meteorological and hydrological parameters on radon emission

The influences of the meteorological (barometric pressure and atmospheric temperature) and hydrological (rainfall and ground water level) parameters are quantified on the soil gas radon emission recorded at the Hsinchu monitoring station, northern Taiwan. In the first instance, the effect of long term trend and seasonal variations were removed by subjecting the recorded time series for the period of September 16, 2009–March 5, 2010 to the digital filter, retaining variations shorter than 30 days. The time series of different parameters were subjected to singular spectrum analysis to decompose the periodic and aperidic variations, which were present in varying strengths in different parameters (Figs. 4 and 5). The reconstructed time series retaining only aperiodic variations account for nearly 70 percent of the total variability of the radon time series, periodic signals corresponding to diurnal and semi- diurnal periods account for less than 2 percent of the variability (Table 1; Fig. 4). Another distinct feature of such decomposition was that random noise present in the radon due to natural or measurement errors were screened out effectively (lower panel in Fig. 4) and thus, reconstructed aperiodic variations simulating bulk feature of observed variations in various parameters (Fig. 6) are ideally suited to search for meteorological/hydrological influences in radon emission. The Influence of barometric pressures and atmospheric temperature on radon variability, estimated using well proven formulation of the BAYTAP-G, are found to be similar, both in amplitude and waveform (Fig. 8). Since time variations in pressure and temperature are not independent of each other and their time evolution has a strong negative correlation, it is difficult to resolve unambiguously whether radon variability is controlled by temperature or pressure variations. Computation of partial correlations show that the influence of pressure on radon is merely the pseudo-effect arising due to the interrelation between temperature and pressure. It has been already shown that temperature inflicted changes radon account for only only about 10–12 percent of the total radon variability (Section 4.1 above). A net consequence is that when deduced aperiodic variations in radon are corrected for temperature induced changes (top panel in Fig. 8), they do not modulate the time variations in radon at station Hsinchu in any significant manner to influence identification and isolation of any earthquake precursor, if present. However, for the purpose of completeness, aperiodic variations in radon corrected for temperature induced changes are used to quantify the nature and extent of the rainfall induced perturbations, which are found to be strong and have a definite diagnostic pattern. Radon at the onset of rainfall shows a step-jump that attain peak with a time lag of 12–15 h. This is attributed to entrapment of soil gas in the top soil cover as increased soil moisture prevents escape of radon into the atmosphere (capping effect). The radon after attaining a peak immediately after the rainfall shows regular recession in a complex manner. Linear decrease or exponential decay, which have been successful in explaining the gravity field and variations ground water head after the long sequences of rainfall, fails to account the decay of radon for several days after the recession of rainfall (Fig. 10a, b). This result is significant, as transportation of one technique successful in explaining the meteorological contamination on one physical parameter may not be applicable to other physical parameters because of differences in the physical mechanism inflicting the influence. Based on the physical consideration, the overall recession in

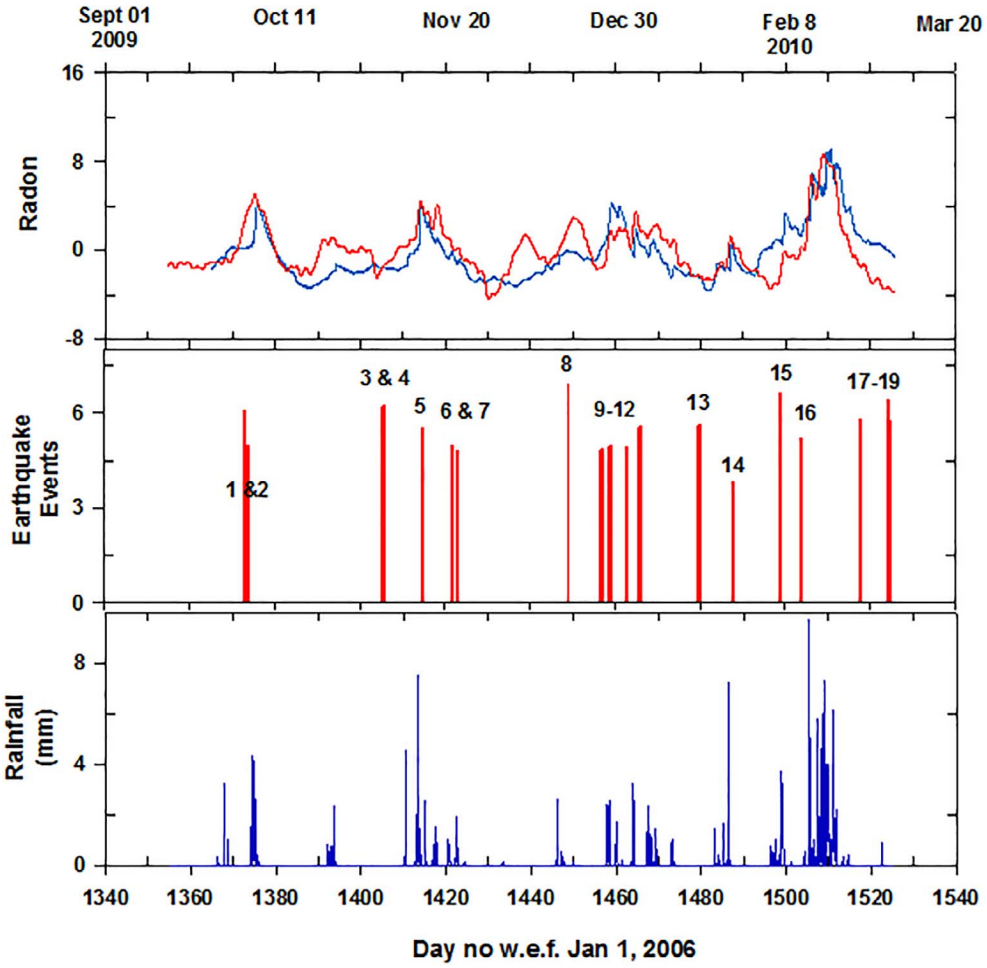

Fig. 11. Plot of deduced decomposed aperiodic variations in radon (red) and simulated radon variations (blue) due to the combined effects of changes in temperature, rainfall occurrences and fluctuations in ground water head at Hsinchu during September 16, 2009 to March 5, 2010. Middle panel shows the timings of 19 earthquakes ($M > 5$) that occurred within a radius of 150 km of radon monitoring station Hsinchu. Lower panel shows the distribution of rainfall (Rf). (For interpretation of the references to color in this figure legend, the reader is referred to the web version of this article.)

radon, after attaining peak soon after the rainfall, is approximated by double exponential decay terms, one corresponding to natural decay of radon with half life of 3.84 days and second representing slow weaken of capping effect after the rainfall (Fig. 10c). The third effect related to internal loading due to rise and fall of groundwater modulate propagation radon in overlying soil layer account for the long term variations in radon, especially in between interval of two sequences of rainfall (Fig. 10d).

5.2. Implications on Identifying earthquake precursors

Despite long years of global research, no universal definition of diagnostic signature of earthquake precursor in radon has emerged. In Taiwan, radon monitoring to search earthquake precursors has largely relied on the identification of characteristic signatures based on the synoptic observations. Continuous monitoring from dense network over a decade has helped to develop a tecto-physical model, wherein the following factors form the guidelines to facilitate detection of precursors in radon (Walia et al., 2009b):

1. Enhancement of radon intensity a few days before the earthquake that maintain elevated levels at least 1–2 days prior to the occurrence of large earthquakes and then return to background level over next few days.
2. Precursory radon changes are in general seen only for earthquakes with
   - Magnitude $M_L \geq 5$ in the representative seismic zone
   - local intensity at radon monitoring station is more than two on the Modified Mercalli intensity scale
   - Focal depth < 40 kms
   - Epicentral distance (R) < 150 kms
   - D/R ratio ≥ 1 (where D is the radius of the preparation zone involved in strain accumulation, estimated using the empirical formula provided by Dobrovolsky et al. (1979) i.e. $D = 10^{0.43M}$ (where M is the Magnitude of impending earthquake). Controlled by regional tectonics, this relationship had been partially modified to and used by many researchers (e.g. Hauksson and Goddard, 1981; Virk, 1996; Walia et al., 2005) for their respective radon data.
3. In case of spatially and temporal clustered earthquakes, the precursory signal is assumed to be related with the largest earthquake
4. Most significantly if precursory signals at three or more radon monitoring stations within the influencing radius of < 150 km are registered, the epicenter is likely to be located in the triangular area defined by the intersection of circles with their center at monitoring stations and radius equal to R (Walia et al., 2013).

It is curious that rainfall inflicted changes in radon have strikingly similar to the nature of perturbations which based on synoptic observations are shown to precede the occurrence of large earthquakes (Fu et al., 2008, 2009; Walia et al., 2009a, 2009b, 2013; Yang et al., 2005, 2006). Fig. 11 gives the plot of radon variations obtained by clubbing the response of meteorological/hydrological (temperature, rainfall and ground water level fluctuations in relation to the aperiodic component deduced from observed radon measurements. During the period of radon data used in the study, some 19 earthquakes with $M \geq 5$ and located within the radius of 150 km from the Hsinchu were reported by CGW. The timings of earthquake occurrences are marked in the middle panel of Fig. 11. One exception being earthquake with $M = 4$ (No. 14) that is included for its proximity and relatively high

local intensity it produced at radon monitoring station Hsinchu. It is curious that rainfall inflicted changes in radon are strikingly similar to the nature of perturbations which based on synoptic observations (point 1 above) are shown to precede the occurrence of large earthquakes (Fu et al., 2008, 2009; Walia et al., 2009a, 2009b, 2013; Yang et al., 2005, 2006). It is also apparent that there is considerable overlap in the timing of earthquake occurrences and rainfall spells shown in the lower panel of Fig. 11. It is found that earthquake No. 5 as well as 14, 15, 16 are accompanied by a rise in radon and hence may qualify to be precursory enhancements, but each increase in radon can more consistently be explained as a steep rise following the rainfall. On the other hand, a significant rise in radon around day numbers 1418 and 1435, when there was no rainfall, could well qualify to be the precursor to the twin earthquakes (No. 6 and 7) and large M6.9 earthquake (No. 8). Similarly the rise in radon on a day no. 1373 that preceded the onset of a strong spell of rainfall may well qualify to be either precursor or coseismic change to earthquakes marked 1 and 2 in Fig. 11. But again the lack of well marked perturbations in association occurrences of a cluster of earthquakes (Nos. 9–13) may be due to mixing of responses from earthquakes and rainfall sequences centered around day nos. 1420 and 1460.

6. Conclusions

Quantitative assessment of the influence of meteorological parameters on the radon intensity at the Hsinchu monitoring station, Taiwan revealed that the temperature/pressure induced variations in radon account for only 10–14 percent of the total variability. The most strong perturbations in radon intensity are seen in association with rainfall sequences. With the onset of the rainfall, radon shows a step-jump that attains peak with a time lag of 12–15 h. Increased soil moisture in the surface soil cover prevents escape of radon into the atmosphere and, thus, increased entrapment of the radon in the top moist cap (capping effect) accounts for the sharp rise following the rainfall. The fast decay of the radon soon after the recession of rainfall is consistent with the natural decay of radon with half life of 3.84 days, whereas slow decay after a lapse of 3–4 days conform to the exponential weakening of the capping effect. In addition, the rise and fall of groundwater head in response to recharge/discharge of the aquifer following the sequence of rainfalls and inventing dry spells modulate propagation of radon in overlying layers, which account for the observed phase shifted long term variations in radon, especially in between interval of two sequences of rainfall (Fig. 10d, e). Comparison of observed and simulated radon variations due to various hydrological parameters (Fig. 11) shows that short term changes inflicted by rainfall events are strikingly similar to the nature of perturbations which based on synoptic observations are shown to precede the occurrence of large earthquakes (Fu et al., 2008, 2009; Walia et al., 2009a, 2009b, 2013; Yang et al., 2005, 2006) and, thus, restrict isolation of possible earthquake precursors from those inflicted by rainfall. An important conclusion to emerge from this case history is that unless the effects of meteorological and hydrological parameters are quantified and eliminated some precursory signals may be either masked or some perturbations may be falsely viewed as earthquake precursors. This strengthens the suggestion of Woith (2015) that only a fraction of reported radon precursors may be real in the sense that they are physically related to the preparation process of an impending earthquake. Much better understanding of the physical processes and the development of robust tools to link likely precursory signal with the source mechanism of earthquakes in the given tectonic setting needs to be pursued before precursory signals can be used in real time forecasting of earthquakes. Recognising the vital knowledge gaps in any individual precursor, the focus of earthquake precursory research is shifting on the integration of multiple precursors (Cicerone et al., 2009; Arora et al., 2012; Zeng et al., 2015)

Acknowledgements

The authors dedicate the present paper to Prof. Tsanyao Frank Yang, the founder of geochemical earthquake precursory research in Taiwan, who left for his heavenly abode in midst of the present study. The authors acknowledge, with thanks the Central Geological Survey of Taiwan (CGS) for funding the establishment of a geochemical monitoring network, alongwith Ministry of Science and Technology (MOST) (earlier know as the National Science Council (NSC)) of Taiwan for partially supporting the network under the projects (NSC 100-2811-M-492-006, NSC 100-2116-M-492-002 & NSC 100-2811-M-492-005). One of us (BRA) thanks the NARL for the award of the Fellowship and to NCREE for hosting and extending excellent facilities during the visit. Authors record their appreciation to Dr. Matsumoto, Geological Survey of Japan for many discussions on the adoption of BAYTAP-G and Space State Decomposition techniques. Authors acknowledge with thanks the critical comments from two anonymous reviewers and the Chief Edior, which helped to improve the manuscript.

References

Allen, M.R., Robertson, A.W., 1996. Distinguishing modulated oscillations fromcoloured noise in multivariate datasets. Clim. Dyn. 12, 775–784.
Arora, B.R., Rawat, W., Kumar, N., Choubey, V.M., 2012. Multi-parameter geophysical observatory: gateway to integrated earthquake precursory research. Curr. Sci. 103 (11), 1286–1299.
Barbosa, S.M., Donner, R.V., Steinitz, G., 2015. Radon applications in geosciences – progress & perspectives. Eur. Phys. J. Spec. Top. 224, 597–603.
Broomhead, D., King, G., 1986. Extracting qualitative dynamics from experi-mental data. Phys. D: Nonlinear Phenomena 20, 217–236.
Cicerone, R.D., Ebel, J.E., Britton, J., 2009. A systematic compilation of earthquake precursors. Tectonophysics 476, 371–396.
Chen, Q., Dam, V.T., Sneeuw, N., Collilieux, X., Weigelt, M., Rebischung, 2013. Singular spectrum analysis for modeling seasonal signals from GPS time series. J. Geodyn. 72, 25–35.
Clements, W.E., Wilkening, M.H., 1974. Atmospheric pressure effects on Rn-222 transport across the earth–air interface. J. Geophys. Res. 79, 5025–5029.
Dobrovolsky, I., Zubkov, S.I., Miachkin, V.I., 1979. Estimation of the size of earthquake preparation zones. Pure Appl. Geophys. 117 (5), 1025–1044.
Finkelstein, M., Eppelbaum, L.V., Price, C., 2006. Analysis of temperature influences on the amplitude–frequency characteristics of Rn gas concentration. J. Environ. Radioact. 86, 251–270.
Fu, C.C., Yang, T.F., Du, J., Walia, V., Chen, Y.G., Liu, T.K., Chen, C.-H., 2008. Variations of helium and radon concentrations in soil gases from an active fault zone in southern Taiwan. Radiat. Meas. 43, S348–S352.
Fu, C.C., Yang, T.F., Walia, V., Liu, T.K., Lin, S.J., Chen, C.-H., Hou, C.S., 2009. Variations of soil-gas composition around the active Chihshang Fault in a plate suture zone, eastern Taiwan. Radiat. Meas. 44, 940–944.
Fujiyoshi, R., Sakamoto, K., Imanishi, T., Sumiyoshi, T., Sawamura, S., Vaupotic, j., Kobal, I., 2006. Meteorological parameters contributing to variabilityin 222Rn activity concentrations in soil gas at a site in Sapporo, Japan. Sci. Total Environ. 370, 224–234.
Ghil, M., Allen, M.R., Dettinger, M.D., Ide, K., Kondrashov, D., Mann, M.E., Robert-son, A.W., Saunders, A., Tian, Y., Varadi, F., Yiou, P., 2002. Advanced spectralmethods for climatic time series. Rev. Geophys. 40 (1), 1003. http://dx.doi.org/10.1029/2000RG000092.
Hartmann, J., Levy, J.K., 2005. Hydrogeological and gas geochemical earthquake precursors: a review for application. Nat. Hazards 34 (3), 279–304.
Heinicke, J., Martinelli, G., Koch, U., 1992. Investigation of the connection between seismicity and CO_2—222Rn content in spring water at the Vogtland area (Germany): first results. In: Abstract, XXIII General Assembly of the European Seismological Commission, Prague.
Hesselbom, A., 1985. Radon in soil gas: a study of methods and instruments for determining radon concentrations in the ground. Geol. Surv. Sweden Ser. C 803, 1–58.
Hauksson, E., Goddard, J.G., 1981. Radon earthquake precursor studies in Iceland. J. Geophys. Res. 86, 7037–7054.
Igarashi, G., Saeki, S., Takahata, N., Sano, Y., 1995. Ground-water radon anomaly before the Kobe earthquake in Japan. Science 269 (5220), 60–61.
Imanishi, Y., Kokubo, K., Tatehata, H., 2006. Effect of underground water on gravity observation at Matsushiro, Japan. J. Geodyn. 41, 221–226.
Jan, C.-D., Chen, T.-H., Lo, W.-C., 2007. Effect of rainfall intensity and distribution on groundwater level fluctuations. J. Hydrol. 332, 348–360.
King, C.Y., Zhang, W., Zhang, Z., 2006. Earthquake induced groundwater and gas changes. Pure Appl. Geophys. 163 (4), 633–645.
Kumar, A., Singh, S., Mahajan, S., Bajwa, B.S., Kalia, R., Dhar, S., 2009. Earthquake precursory studies in Kangra valley of North West Himalayas, India, with special emphasis on radon emission. Appl. Radiat. Isot. 67, 1904–1911.
Kumar, A., Walia, V., Arora, B.R., Yang, T.F., Lin, S.-J., Fu, C.-C., Chen, C.-H., Wen, K.-L., 2015. Identifications and removal of diurnal and semi-diurnal variations in radon

time-series data of Hsinhua monitoring station in SW Taiwan using singular spectrum analysis. Nat. Hazards 79 (1), 317–330.
Matsumoto, N., 1992. Regression analysis for anomalous changes of ground water level due to earthquakes. Geophys. Res. Lett. 119, 1193–1196.
Matsumoto, N., Kitagawa, G., Roeloffs, E.A., 2003. Hydrological response to earthquakes in the Haibara well, central Japan – I. Groundwater level changes revealed using state space decomposition of atmospheric pressure, rainfall and tidal responses. Geophys. J. Int. 155 (3), 885–898.
Naujoks, M., Kroner, C., Weise, A., Jahr, T., Krause, Eisner, S., 2010. Evaluating local hydrological modelling by temporal gravity observations and a gravimetric three-dimensional model. Geophys. J. Int. 182 (1), 233–249.
Nawa, K., Suda, N., Yamada, I., Miyajima, R., Okubo, S., 2009. Coseismic change and precipitation effect in temporal gravity variation at Inuyama, Japan: a case of the 2004 off the Kii peninsula earthquakes observed with a superconducting gravimeter. J. Geodyn. 48 (1), 1–5.
Plaut, G., Vautard, R., 1994. Spells of low-frequency oscillations and weather regimesin the northern hemisphere. J. Atmos. Sci. 51, 210–236.
Scholz, C.H., Sykes, L.R., Aggarwal, Y., 1973. Earthquake prediction: a physical basis. Science 181, 803–810.
Schumann, R.R., Owen, D.E., Asher-Bolinder, S., 1988. Weather factors affecting soil gas radon concentrations at a single site in the semiarid western U.S. In: Proceedings of the 1988 EPA Symposium on Radon and Radon Reduction Technology, vol. 2, no. 3, pp. 1–13.
Schumann, R.R., Owen, D.E., Asher, B.S., 1992. Effects of weather and soil characteristics on temporal variations in soil–gas radon concentrations. Geol. Soc. Am. 271, 65–72.
Steinitz, G., Begin, Z.B., Gazit-Yaari, N., 2003. A statistically significant relation between Rn flux and weak earthquakes in the Dead Sea rift valley. Geology 31, 505–508.
Toutain, J., Baubron, J.C., 1999. Gas geochemistry and seismotectonics: a review. Tectonophysics 304, 1–27.
Thomas, D.M., 1988. Geochemical precursors to earthquake. Pure Appl. Geophys. 126, 241–265.
Ulomov, V.I., Mavashev, B.Z., 1967. A precursor of a strong tectonic earthquake. Academy Science. USSR Earth Sci. Sect. 176, 9–11.
Vautard, R., Yiou, Ghil, M., 1992. Singular-spectrum analysis: a toolkit forshort, noisy chaotic signals. Phys. D: Nonlinear Phenomena 58, 95–126.
Vautard, R., Ghil, M., 1989. Singular spectrum analysis in nonlinear dynamics, with applications to paleoclimatic time series. Phys. D: Nonlinear Phenomena 35, 395–424.
Virk, H.S., 1996. A critique of empirical scaling relationship between earthquake magnitude, epicentral distance and precursor time for interpretation of radon data. J. Earthq. Predict. Res. 5, 574–583.
Virk, H.S., Walia, V., Kumar, N., 2001. Helium/radon precursory anomalies of Chamoli earthquake, Garhwal Himalaya, India. J. Geodyn. 31, 201–210.
Tamura, Y., Sato, T., Ooe, M., Ishiguro, M., 1991. A procedure for tidal analysis with a Bayesian information criterion. Geophys. J. Int. 104, 507–516.
Walia, V., Virk, H.S., Yang, T.F., Mahajan, S., Walia, M., Bajwa, B.S., 2005. Earthquake prediction studies using radon as a precursor in N-W Himalayas, India: a case study. Terrestrial Atmos. Oceanic Sci. 16 (4), 775–804.
Walia, V., Yang, T.F., Lin, S.J., Hong, W.L., Fu, C.C., Wen, K.L., Chen, C.H., 2009a. Geochemical variation of soil-gas composition for fault and earthquake precursory studies along Hsincheng fault in NW Taiwan. Appl. Radiat. Isot. 67, 1855–1863.
Walia, V., Yang, T.F., Lin, S.J., Hong, W.L., Fu, C.C., Wen, K.L., Chen, C.H., 2009b. Continuous temporal soil.gas composition variations for earthquake precursory studies along Hsincheng and Hsinhua faults in Taiwan. Radiat. Meas. 44 (934), 939.
Walia, V., Yang, T.F., Lin, S.-J., Kumar, A., Fu, C.C., Chiu, J.-M., Chang, H.-H., Wen, K.-L., Chen, C.-H., 2013. Temporal variation of soil gas compositions for earthquake surveillance in Taiwan. Radiat. Meas. 50, 154–159.
Wakita, H., Nakamura, Y., Sano, Y., 1988. Short-term and intermediate-term geochemical precursors. Pure Appl. Geophys. 126 (2–4), 267–278.
Woith, H., 2015. Radon earthquake precursor: a short review. Eur. Phys. J. Spec. Top. 224 (4), 611–627.
Yang, T.F., Walia, V., Chyi, L.L., Fu, C.C., Chen, C.-H., Liu, T.K., Song, C.S., Lee, R.Y., Lee, M., 2005. Variations of soil radon and thoron concentrations in a fault zone and prospective earthquakes in SW Taiwan. Radiat. Meas. 40, 496–502.
Yang, T.F., Fu, C.C., Walia, V., Chen, C.-H., Chyi, L.L., Liu, T.K., Song, S.R., Lee, M., Lin, C.W., Lin, C.C., 2006. Seismo-geochemical variations in SW Taiwan: multiparameter automatic gas monitoring results. Pure Appl. Geophys. 163, 693–709.
Zeng, X., Lin, Y., Chen, W., Bai, Z., Liu, J.-Y., Chen, C.-H., 2015. Multiple seismo-anomalies associated with the M6.1 Ludian earthquake on August 3, 2014. J. Asian Earth Sci. 114, 352–361.
Zmazek, B., Zivcic, M., Todorovski, L., Dzeroski, S., Vaupotic, J., Kobal, I., 2005. Radon in soil gas: how to identify anomalies caused by earthquakes. Appl. Geochem. 20, 1106–1119.